Robotica (2015) volume 33, pp. 1099–1112. © Cambridge University Press 2014
doi:10.1017/S0263574714001465

A persistent method for parameter identification of a seven-axes manipulator

Matthias Neubauer*, Hubert Gattringer and Hartmut Bremer

Institute for Robotics, Johannes Kepler University, Linz 4040, Austria

(Accepted May 13, 2014. First published online: June 13, 2014)

SUMMARY

This paper presents a persistent method for the identification problem of open-chained robotic systems. Based on the Projection Equation, a new, direct method to collect the dynamic and friction parameters in linear form is worked out. However, in this form, linear dependencies in the parameters occur and they are canceled out with the help of the QR algorithm. The obtained linear independent parameters are the base parameters of the system. To ensure a good excitation, the identification is improved by using optimized trajectories defined by Fourier-series, taking also physical constraints into account. The evaluation of the dynamic robot parameters is realized with a least squares error optimization. Furthermore, the result strongly depends on a special choice of weighting matrices for the error. Experimental results for a seven-axes robotic system (standard six-axes industrial manipulator mounted on a linear axis) are presented in detail. Additionally, the influence of temperature effects to base parameter changes is discussed.

KEYWORDS: Industrial robots; Dynamic modeling; Parameter identification.

1. Introduction

In modern industry the applications are getting faster and faster and therefore the desire for fast robots without a loss of accuracy arises. To handle the high dynamic movements, conventional linear control concepts often fail, this leads to nonlinear model-based control strategies, for instance, computed-torque or model predictive control. Essential for the design and evaluation of the controller is an accurate dynamic model of the system. Clearly, the containing parameters are very important and thus an identification is indispensable.

The derivation of the dynamic model of rigid body systems is a well-known topic and can be found in several classical robotic publications, such as refs. [3], [7], [19] and [18]. All of these methods have in common, that a reformulation of the dynamic model to a linear form in the parameter range is required. Unfortunately, not all of the parameters can be individually separated nor uniquely identified. Thus a classification in independent, linear-dependent, and unidentifiable parameters has to be worked out. A manual classification is possible but is time consuming and not universal applicable. Other researchers have presented routines to automatically evaluate the identifiable parameters, like those of ref. [13], who discussed a reformulation of a Lagrangian dynamic model or of ref. [14], who published a procedure based on the Newton–Euler formulation. In contrary to these contributions, we present a direct method for deriving the dynamic model by using the Projection Equation, see ref. [5], and getting a linear system with respect to the dynamic parameters. With a succeeding QR decomposition, linear independent base parameters of the robot can be calculated automatically. These parameters can be identified with a least squares minimization, as discussed widely in ref. [12] or [15]. Still, the identification can be done in various ways; especially the collection of measurements is an important and challenging task. The publication of ref. [1] depicts the benefits of a single-axis identification. However, the focus there was to identify the parameters of a flexible robot including

* Corresponding author. E-mail: matthias.neubauer_1@jku.at

https://doi.org/10.1017/S0263574714001465 Published online by Cambridge University Press

joint stiffness parameters. Nevertheless, disassembling a robot is often unwanted or even impossible. An alternative solution is a stepwise identification of each axis, discussed accurately in the book, in ref. [15]. Contrary to these stepwise techniques, their exist several publications dealing with a system identification at once, e.g., ref. [21]. A comparison between a stepwise and overall identification is addressed in ref. [4]. Also a splitting of the identification, by pre-computing the friction parameters using an integral model is possible, see ref. [16]. In this context, also different strategies for the trajectory generation arise. For instance, the paper in ref. [17] calculates trajectories according to the gradient of the covariance matrix of the succeeding least squares optimization, or refs. [10] and [2], discuss the calculation of optimal identification points followed by a fitting procedure in order to get joint trajectories. However, in this contribution a method presented in ref. [8], [21] or [6], where a parameterization of the joint trajectories by Fourier series and a nonlinear optimization in order to calculate optimal trajectories is used. Regarding the parameter evaluation, new scientific findings are achieved by introducing a weighting of the error according to characteristic parameters of the robot. Thus, the identification with least squares minimization, which fails for the tested scenario without a weighting, can be applied and reliable parameters are obtained.

Hence, Section 2 discusses the derivation of the dynamic model with special emphasis regarding the requirements of the identification process. Thereafter, the robot, on which the identification is applied, is introduced. Subsequently, linear dependencies between the parameters are eliminated by a QR decomposition and thus the independent base parameters of the system are calculated. Section 4 deals with the identification of the parameters using least squares optimization and optimal excitation trajectories. Thereafter, the resultant parameters are discussed and verified by experimental results. Also, temperature changes, which appear during the start up of the robot, are analyzed and there effects on the dynamic behavior are shown. Finally, the reduction of the computation time, achieved by using base parameters for model-based feed-forward control is presented.

2. Modeling

Throughout this paper we consider rigid body systems with n number of bodies. To obtain the equations of motion the Projection Equation

$$\sum_{i=1}^{n} \left[\left(\frac{\partial \mathbf{v}_c}{\partial \dot{\mathbf{q}}} \right)^T \left(\frac{\partial \boldsymbol{\omega}_c}{\partial \dot{\mathbf{q}}} \right)^T \right]_i \left[\begin{matrix} \dot{\mathbf{p}} + \tilde{\boldsymbol{\omega}}_{IB}\, \mathbf{p} - \mathbf{f}^e \\ \dot{\mathbf{L}} + \tilde{\boldsymbol{\omega}}_{IB}\, \mathbf{L} - \mathbf{M}^e \end{matrix} \right]_i = 0, \tag{1}$$

see ref. [5], is used. The vector $\mathbf{q}$ describes the generalized coordinates and the linear $\mathbf{p}$ and angular momenta $\mathbf{L}$ are given by

$$\begin{pmatrix} \mathbf{p} \\ \mathbf{L} \end{pmatrix} = \begin{bmatrix} m\,\mathbf{I} & 0 \\ 0 & \mathbf{J}^c \end{bmatrix} \begin{pmatrix} \mathbf{v}_c \\ \boldsymbol{\omega}_c \end{pmatrix}, \tag{2}$$

with mass m, identity matrix $\mathbf{I}$, and the inertia tensor $\mathbf{J}^c$. Note, the index c represents the center of gravity and the cross product for vectors $\mathbf{a} \times \mathbf{b}$ is denoted by $\tilde{\mathbf{a}}\,\mathbf{b}$. Furthermore, the vectors which belong to body i are represented in their body fixed coordinate system B ($\boldsymbol{\omega}_{IB}$—rotational velocity of the coordinate system B). In general, the Projection Equation allows arbitrary coordinate systems for each body, but for our purpose a body fixed frame is used. Thus, $\boldsymbol{\omega}_{IB} = \boldsymbol{\omega}_c$ and the skew-symmetric matrix $\tilde{\boldsymbol{\omega}}_{IB}$ follows to

$$\tilde{\boldsymbol{\omega}}_{IB} = \tilde{\boldsymbol{\omega}}_c = \begin{bmatrix} 0 & -\omega_z & \omega_y \\ \omega_z & 0 & -\omega_x \\ -\omega_y & \omega_x & 0 \end{bmatrix}. \tag{3}$$

Vectors $\mathbf{f}^e$ and $\mathbf{M}^e$ describe the impressed forces and torques. Substituting Eq. (2) into Eq. (1) we get

$$\sum_{i=1}^{n} \mathbf{F}_{c,i}^T \left\{ \begin{bmatrix} m\,\mathbf{I} & 0 \\ 0 & \mathbf{J}^c \end{bmatrix} \begin{pmatrix} \dot{\mathbf{v}}_c \\ \dot{\boldsymbol{\omega}}_c \end{pmatrix} + \begin{bmatrix} \tilde{\boldsymbol{\omega}}_{IB}\, m & 0 \\ 0 & \tilde{\boldsymbol{\omega}}_{IB}\, \mathbf{J}^c \end{bmatrix} \begin{pmatrix} \mathbf{v}_c \\ \boldsymbol{\omega}_c \end{pmatrix} - \begin{pmatrix} \mathbf{f}^e \\ \mathbf{M}^e \end{pmatrix} \right\}_i = 0, \tag{4}$$

https://doi.org/10.1017/S0263574714001465 Published online by Cambridge University Press

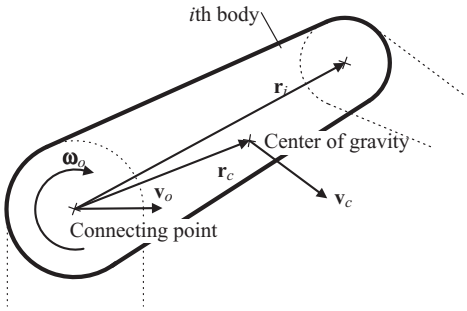

Fig. 1. Sketch of body i.

where

$$\mathbf{F}_{c,i}^T = \left[\left(\frac{\partial \mathbf{v}_c}{\partial \dot{\mathbf{q}}} \right)^T \quad \left(\frac{\partial \boldsymbol{\omega}_c}{\partial \dot{\mathbf{q}}} \right)^T \right]_i \tag{5}$$

is the appropriate Jacobian for the projection in the minimal space. Because the measurements for the identification are taken in the joints, Eq. (4) has to be reformulated. Therefore, we define the velocities of the center of gravity w.r.t. the joint velocities leading to

$$\begin{pmatrix} \mathbf{v}_c \\ \boldsymbol{\omega}_c \end{pmatrix}_i = \begin{bmatrix} \mathbf{I} & \tilde{\mathbf{r}}_c^T \\ 0 & \mathbf{I} \end{bmatrix}_i \begin{pmatrix} \mathbf{v}_o \\ \boldsymbol{\omega}_o \end{pmatrix}_i , \tag{6}$$

with $\mathbf{v}_o$ the translational and $\boldsymbol{\omega}_o$ the angular velocity of the connecting point of the link. Note, because only rigid bodies are considered, $\boldsymbol{\omega}_o = \boldsymbol{\omega}_c$. The vector $\mathbf{r}_c$ describes the center of gravity w.r.t. the connecting point (see Fig. 1). Hence, Eq. (5) follows to

$$\mathbf{F}_{c,i} = \begin{bmatrix} \frac{\partial \mathbf{v}_c}{\partial \dot{\mathbf{q}}} \\ \frac{\partial \boldsymbol{\omega}_c}{\partial \dot{\mathbf{q}}} \end{bmatrix}_i = \begin{bmatrix} \mathbf{I} & \tilde{\mathbf{r}}_c^T \\ 0 & \mathbf{I} \end{bmatrix}_i \underbrace{\begin{bmatrix} \frac{\partial \mathbf{v}_o}{\partial \dot{\mathbf{q}}} \\ \frac{\partial \boldsymbol{\omega}_o}{\partial \dot{\mathbf{q}}} \end{bmatrix}_i}_{\mathbf{F}_{o,i}} . \tag{7}$$

Substituting Eqs. (6) and (7) into (4), we get

$$\sum_{i=1}^{n} \mathbf{F}_{o,i}^T \left\{ \begin{bmatrix} m\,\mathbf{I} & m\,\tilde{\mathbf{r}}_c^T \\ m\,\tilde{\mathbf{r}}_c & \mathbf{J}^o \end{bmatrix} \begin{pmatrix} \dot{\mathbf{v}}_o \\ \dot{\boldsymbol{\omega}}_o \end{pmatrix} + \begin{bmatrix} \tilde{\boldsymbol{\omega}}_o\, m & \tilde{\boldsymbol{\omega}}_o\, \tilde{\mathbf{r}}_c^T\, m \\ \tilde{\mathbf{r}}_c\, \tilde{\boldsymbol{\omega}}_o\, m & \tilde{\boldsymbol{\omega}}_o\, \mathbf{J}^o \end{bmatrix} \begin{pmatrix} \mathbf{v}_o \\ \boldsymbol{\omega}_o \end{pmatrix} - \begin{bmatrix} \mathbf{I} & 0 \\ \tilde{\mathbf{r}}_c & \mathbf{I} \end{bmatrix} \begin{pmatrix} m\,\mathbf{g} \\ 0 \end{pmatrix} \right\}_i = \mathbf{Q}^o, \tag{8}$$

where $\mathbf{J}^o = \mathbf{J}^c + m\,\tilde{\mathbf{r}}_c\,\tilde{\mathbf{r}}_c^T$ describes the inertia tensor w.r.t. the connecting point and $\mathbf{Q}^o$ the generalized forces except the already included gravitational force $\mathbf{f}^e = m\,\mathbf{g}$. Note, the gravitational force is represented in the body fixed frame B. In order to extract the dynamic parameters we rearrange the vector $\mathbf{J}^o\,\boldsymbol{\omega}_o$ and get

$$\mathbf{J}^o\,\boldsymbol{\omega}_o = \begin{bmatrix} A & -F & -E \\ -F & B & -D \\ -E & -D & C \end{bmatrix} \begin{pmatrix} \omega_x \\ \omega_y \\ \omega_z \end{pmatrix} = \left[\underbrace{\begin{array}{ccc} \omega_x & 0 & 0 \\ 0 & \omega_y & 0 \\ 0 & 0 & \omega_z \end{array}}_{\boldsymbol{\Omega}} \; \underbrace{\begin{array}{ccc} 0 & -\omega_z & -\omega_y \\ -\omega_z & 0 & -\omega_x \\ -\omega_y & -\omega_x & 0 \end{array}}_{-\hat{\boldsymbol{\Omega}}} \right] \underbrace{\begin{pmatrix} A \\ B \\ C \\ D \\ E \\ F \end{pmatrix}}_{\mathbf{j}} . \tag{9}$$

https://doi.org/10.1017/S0263574714001465 Published online by Cambridge University Press

Parameter vector $\mathbf{j}$ contains the moments of inertia. Similar to Eq. (9), also the other dynamic parameters (m, $m\,\mathbf{r}_c$) of Eq. (8) are isolated, leading to

$$\sum_{i=1}^{n} \mathbf{F}_{o,i}^T \left\{ \begin{bmatrix} \dot{\mathbf{v}}_o & \dot{\tilde{\boldsymbol{\omega}}}_o & 0 \\ 0 & -\dot{\tilde{\mathbf{v}}}_o & (\dot{\boldsymbol{\Omega}}|\, - \dot{\hat{\boldsymbol{\Omega}}}) \end{bmatrix} \begin{pmatrix} m \\ m\,\mathbf{r}_c \\ \mathbf{j} \end{pmatrix} + \begin{bmatrix} \tilde{\boldsymbol{\omega}}_o\,\mathbf{v}_o & \tilde{\boldsymbol{\omega}}_o\,\tilde{\boldsymbol{\omega}}_o & 0 \\ 0 & -(\tilde{\boldsymbol{\omega}}_o\,\mathbf{v}_o)^{\tilde{}} & \tilde{\boldsymbol{\omega}}_o\,(\boldsymbol{\Omega}|\, - \hat{\boldsymbol{\Omega}}) \end{bmatrix} \begin{pmatrix} m \\ m\,\mathbf{r}_c \\ \mathbf{j} \end{pmatrix} - \begin{bmatrix} \mathbf{g} & 0 & 0 \\ 0 & -\tilde{\mathbf{g}} & 0 \end{bmatrix} \begin{pmatrix} m \\ m\,\mathbf{r}_c \\ \mathbf{j} \end{pmatrix} \right\}_i = \mathbf{Q}^o\,. \tag{10}$$

Thus, we get a linear system of equations w.r.t. the parameter vector $\mathbf{p}_i = [m \quad m\,\mathbf{r}_c^T \quad \mathbf{j}^T]_i^T$ of each body i. Furthermore, in combination with the projection matrix $\mathbf{F}_{o,i}$ and the succeeding summation, we obtain the equations of motion for our multi-body system

$$\sum_{i=1}^{n} \underbrace{\mathbf{F}_{o,i}^T\,\overline{\boldsymbol{\Theta}}_i}_{\boldsymbol{\Theta}_i}\,\mathbf{p}_i = \mathbf{Q}^o\,. \tag{11}$$

For simplicity, we only consider inertia matrices with principal axes, thus D, E, and F are canceled (see Eq. (9)) leading to

$$\overline{\boldsymbol{\Theta}}_i = \begin{bmatrix} \dot{\mathbf{v}}_o + \tilde{\boldsymbol{\omega}}_o\,\mathbf{v}_o - \mathbf{g} & \dot{\tilde{\boldsymbol{\omega}}}_o + \tilde{\boldsymbol{\omega}}_o\,\tilde{\boldsymbol{\omega}}_o & 0 \\ 0 & -(\dot{\mathbf{v}}_o + \tilde{\boldsymbol{\omega}}_o\,\mathbf{v}_o - \mathbf{g})^{\tilde{}} & \dot{\boldsymbol{\Omega}} + \tilde{\boldsymbol{\omega}}_o\,\boldsymbol{\Omega} \end{bmatrix}. \tag{12}$$

Hence, all inertia and gravitational forces of a rigid body system are included. To model joint friction, additional forces $\mathbf{Q}_v$ for viscous friction and $\mathbf{Q}_c$ for Coulomb friction are introduced. Viscous friction is considered by

$$\begin{aligned} \mathbf{Q}_v &= -\boldsymbol{\Theta}_v \underbrace{\begin{pmatrix} d_{v,1} \\ \vdots \\ d_{v,n} \end{pmatrix}}_{\mathbf{p}_v} \\ \boldsymbol{\Theta}_v &= \operatorname*{diag}_{i=1\ldots n} \{\dot{q}_i\} \end{aligned} \tag{13}$$

and Coulomb friction by

$$\begin{aligned} \mathbf{Q}_c &= -\boldsymbol{\Theta}_c \underbrace{\begin{pmatrix} d_{c,1} \\ \vdots \\ d_{c,n} \end{pmatrix}}_{\mathbf{p}_c} \\ \boldsymbol{\Theta}_c &= \operatorname*{diag}_{i=1\ldots n} \left\{ \tanh\left(\frac{\dot{q}_i}{\epsilon_c} \right) \right\}. \end{aligned} \tag{14}$$

Note, the sign function which is typically used for modeling Coulomb friction is approximated by a tan h with a ϵ_c of 0.01. Now substituting $\mathbf{Q}^o$ in Eq. (11) by

$$\mathbf{Q}^o = \mathbf{Q}_v + \mathbf{Q}_c + \mathbf{Q}_m \tag{15}$$

https://doi.org/10.1017/S0263574714001465 Published online by Cambridge University Press

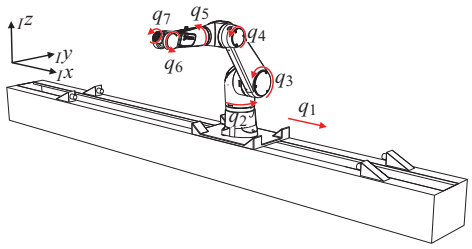

Fig. 2. Degrees of freedom of the robot.

with $\mathbf{Q}_m$ as the remaining generalized forces, we finally get

$$\begin{aligned}
[\boldsymbol{\Theta}_1 \quad \ldots \quad \boldsymbol{\Theta}_n \quad \boldsymbol{\Theta}_v \quad \boldsymbol{\Theta}_c] \begin{pmatrix} \mathbf{p}_1 \\ \vdots \\ \mathbf{p}_n \\ \mathbf{p}_v \\ \mathbf{p}_c \end{pmatrix} &= \mathbf{Q}_m \\
\boldsymbol{\Theta}\,(\mathbf{q}, \dot{\mathbf{q}}, \ddot{\mathbf{q}})\ \mathbf{p} &= \mathbf{Q}_m\,.
\end{aligned} \tag{16}$$

Thus far, we have found a method for deriving the equations of motion which lead to a linear system w.r.t. the dynamic parameters $\mathbf{p}$. Besides, each body is represented by nine parameters, seven according to inertia and two to model friction. Furthermore, we assumed that the geometric parameters, like l_{i_x}, l_{i_y}, and l_{i_z} which appear in the connection vector $\mathbf{r}_i = [l_{i_x}\ l_{i_y}\ l_{i_z}]^T$ (see Fig. 1) for each body, are known.

3. Industrial Robot

Now the general method of Section 2 is applied to our specific robot to discuss the details for a physical robotic system. The used robot consists of an ordinary six-axes industrial manipulator from Stäubli (TX90L) and is mounted on top of a linear axis. Figure 2 shows the robot with the generalized coordinates $\mathbf{q} = [q_1 \quad q_2 \quad q_3 \quad q_4 \quad q_5 \quad q_6 \quad q_7]^T$ and the orientation of the inertial frame I. Because of 7 degrees of freedom, also seven rigid bodies are considered. Overall 49 parameters according to inertia forces and 14 parameters for viscous and Coulomb friction are introduced. Thus far, the inertia of the motors are not included. For simplicity and because the inertia of the motors are assumed to be small, only the term

$$\begin{aligned}
\mathbf{Q}_{I,m} &= \boldsymbol{\Theta}_{I,m}\,\mathbf{p}_{I,m} \\
\boldsymbol{\Theta}_{I,m} &= \operatorname*{diag}_{k=1\ldots7} \{\ddot{q}_k\} \\
\mathbf{p}_{I,m}^T &= \left[i_{G1}^2\, C_{M,1} \quad \ldots \quad i_{G7}^2\, C_{M,7}\right]
\end{aligned} \tag{17}$$

with the gear ratios i_{Gk} and the moment of inertia of the motor shafts $C_{M,k}$ for $k = 1, \ldots, 7$ are added. Note, other terms for the motors are not considered since they are of magnitudes smaller and do therefore not influence the dynamics. Doing so, another seven parameters are introduced and by adding Eqs. (17) to (16) we get

$$\begin{aligned}
\left[\boldsymbol{\Theta}_1 \quad \ldots \quad \boldsymbol{\Theta}_7 \quad \boldsymbol{\Theta}_v \quad \boldsymbol{\Theta}_c \quad \boldsymbol{\Theta}_{I,m}\right] \begin{pmatrix} \mathbf{p}_1 \\ \vdots \\ \mathbf{p}_7 \\ \mathbf{p}_v \\ \mathbf{p}_c \\ \mathbf{p}_{I,m} \end{pmatrix} &= \mathbf{Q}_m \\
\boldsymbol{\Theta}\,(\mathbf{q}, \dot{\mathbf{q}}, \ddot{\mathbf{q}})\ \mathbf{p} &= \mathbf{Q}_m\,.
\end{aligned} \tag{18}$$

https://doi.org/10.1017/S0263574714001465 Published online by Cambridge University Press

The generalized forces $\mathbf{Q}_m$ are given by

$$\mathbf{Q}_m^T = \begin{bmatrix} i_{G1}\, M_1 & \dots & i_{G7}\, M_7 \end{bmatrix}, \tag{19}$$

where M_k for $k = 1, \dots, 7$ are the motor torques. Finally, 70 unknown parameters describe the dynamic system of our robot. Almost always, and here as well, not all the parameters in $\mathbf{p}$ are independent, and thus Eq. (18) has to be reformulated. In general there exist symbolic or numerical approaches to obtain the independent parameters. A symbolic method for tree structured robots is provided by ref. [13]. The two main numerical approaches are based on a singular value decomposition (SVD) or a QR decomposition and are discussed in ref. [9]. To achieve a quick and automatically calculated solution, we use a QR decomposition. Therefore, $\mathbf{\Theta}$ is evaluated 25 times with random joint values (position, velocity, and acceleration) and stacked into a new matrix called $\mathbf{\Theta}_{QR}$. Then the QR decomposition is carried out leading to

$$\begin{aligned} \mathbf{\Theta}_{QR} &= \overline{\mathbf{Q}}\,\overline{\mathbf{R}} \\ \overline{\mathbf{Q}}^T\,\mathbf{\Theta}_{QR} &= \overline{\mathbf{R}} \end{aligned} \tag{20}$$

with the orthonormal matrix $\overline{\mathbf{Q}} \in \mathbb{R}^{25\times 7,70}$ and the upper triangular matrix $\overline{\mathbf{R}} \in \mathbb{R}^{70,70}$. Every parameter l, where the element of $\overline{\mathbf{R}}_{l,l}$ is zero is not identifiable and the corresponding column l of $\mathbf{\Theta}$ is collected in $\hat{\mathbf{\Theta}}_2$, the rest is combined in $\hat{\mathbf{\Theta}}_1$. Now we obtain

$$\begin{bmatrix} \hat{\mathbf{\Theta}}_1 & \hat{\mathbf{\Theta}}_2 \end{bmatrix} \begin{pmatrix} \mathbf{p}_1 \\ \mathbf{p}_2 \end{pmatrix} = \mathbf{Q}_m, \tag{21}$$

with $\mathbf{p}_1$ the independent and $\mathbf{p}_2$ the dependent parameters. By substituting $\hat{\mathbf{\Theta}}_2 = \hat{\mathbf{\Theta}}_1 \boldsymbol{\kappa}$ (parameters are linear dependent) the identification problem follows to

$$\hat{\mathbf{\Theta}}_1 \underbrace{(\mathbf{p}_1 + \boldsymbol{\kappa}\, \mathbf{p}_2)}_{\mathbf{p}_B} = \mathbf{Q}_m, \tag{22}$$

where $\mathbf{p}_B$ are the identifiable base parameters. $\hat{\mathbf{\Theta}}_1$ contains the linear independent part from $\mathbf{\Theta}$.

For our robot, 44 identifiable parameters are found and we finally get

$$\underbrace{\hat{\mathbf{\Theta}}_1 \left(\mathbf{q}^{(k)},\, \dot{\mathbf{q}}^{(k)},\, \ddot{\mathbf{q}}^{(k)}\right)}_{\mathbf{\Theta}_B^{(k)}} \mathbf{p}_B = \underbrace{\mathbf{Q}_m}_{\mathbf{Q}^{(k)}}, \tag{23}$$

with $\mathbf{\Theta}_B^{(k)} \in \mathbb{R}^{7,44}$, $\mathbf{p}_B \in \mathbb{R}^{44}$, and $\mathbf{Q}^{(k)} \in \mathbb{R}^7$. The introduced superscript (k) denotes the used values for the evaluation and will become important in the next section. Exemplarily, for our robot the first two base parameters are

$$\begin{aligned} \mathbf{p}_B(1) &= m_1 + m_2 + m_3 - \frac{1}{l_{3_z}} (m_4\, r_{c,4_z}) + i_{G1}^2\, C_{M,1}, \\ \mathbf{p}_B(2) &= m_2\, r_{c,2_x} + l_{2_x}\, m_3 - \frac{l_{2_x}}{l_{3_z}} (m_4\, r_{c,4_z}), \end{aligned} \tag{24}$$

where $m_2\, r_{c,2_x}$ represents the x-component of the vector $m\, \mathbf{r}_c$ of the 2nd body and similarly $m_4\, r_{c,4_z}$ is the z-component of $m\, \mathbf{r}_c$ of the 4th body. Also worth mentioning is that all parameters of the viscous

https://doi.org/10.1017/S0263574714001465 Published online by Cambridge University Press

and Coulomb friction appear as base parameters, e.g.,

$$\begin{aligned}\mathbf{p}_B(27) &= d_{v,1,}\\ \mathbf{p}_B(28) &= d_{v,2,}\\ \mathbf{p}_B(34) &= d_{c,1,}\\ \mathbf{p}_B(35) &= d_{c,2}.\end{aligned}$$

To get the base parameters in a symbolic notation like Eq. (24), after using a numerical method to calculate $\boldsymbol{\kappa}$ in Eq. (22), a manual and thus time-consuming analysis of the base parameters is needed. But, since a symbolic representation is not required for the identification, the manual classification can be canceled, and thus it is not a notable drawback of the presented procedure.

4. Identification

In this section the evaluation of the parameters is shown. Basis for the identification process are measurements of the joint angles, velocities, accelerations, and the corresponding motor torques. Because only the joint angles are measured, the velocities and accelerations have to be calculated. The time derivatives of the joint values are approximated by a filter with the transfer function

$$G(s) = \frac{s}{\frac{s}{\omega_f} + 1}. \tag{25}$$

Note, the discrete version of $G(s)$ is used with $\omega_f = 1200\,\mathrm{rad/s}$ for obtaining the joint velocities. To calculate the accelerations, we set $\omega_f = 100\,\mathrm{rad/s}$ and applied the filter in forward and reverse directions to obtain a zero-phase filtered signal, see ref. [12]. For every sample value of the trajectory, Eq. (23) is evaluated and stacked leading to

$$\underbrace{\begin{pmatrix}\boldsymbol{\Theta}_B^{(1)}\\ \vdots\\ \boldsymbol{\Theta}_B^{(N)}\end{pmatrix}}_{\boldsymbol{\Theta}_B}\mathbf{p}_B = \underbrace{\begin{pmatrix}\mathbf{Q}^{(1)}\\ \vdots\\ \mathbf{Q}^{(N)}\end{pmatrix}}_{\mathbf{Q}} \tag{26}$$

with N is the number of samples.

4.1. Least squares optimization

Due to measurement as well as modeling errors and because of the overdeterminacy of Eq. (26), an error $\mathbf{e}$ is introduced and defined to

$$\mathbf{e} = \boldsymbol{\Theta}_B\,\mathbf{p}_B - \mathbf{Q}. \tag{27}$$

According to refs. [12] and [20] the parameter vector $\mathbf{p}_B$ can be calculated by solving a minimum least squares optimization with the cost functional

$$\mathcal{L}(\mathbf{p}_B) = \frac{1}{2}\,\mathbf{e}^T\,\mathbf{e}\,. \tag{28}$$

For our robot this cost functional yields to an unsatisfying solution, because each element of the error $\mathbf{e}$ is treated equally. Due to the construction of our robot, the maximum torque of each axis is quite different, e.g., the maximum motor torque $M_{1,\max} = 69\,\mathrm{N\,m}$ and $M_{7,\max} = 2.2\,\mathrm{N\,m}$. Hence, the error has to be weighted. Therefore we enhance Eq. (27) with a weighting matrix $\mathbf{W}$ leading to

$$\hat{\mathbf{e}} = \mathbf{W}\,\underbrace{(\boldsymbol{\Theta}_B\,\mathbf{p}_B - \mathbf{Q})}_{\mathbf{e}}, \tag{29}$$

https://doi.org/10.1017/S0263574714001465 Published online by Cambridge University Press

where $\mathbf{W}$ is a block-diagonal matrix, defined as

$$\begin{aligned} \mathbf{W} &= \underset{k=1,\ldots,N}{\text{diag}} \left\{ \mathbf{W}^{(k)} \right\}, \\ \mathbf{W}^{(k)} &= \underset{j=1,\ldots,7}{\text{diag}} \left\{ \frac{1}{i_{Gj}\, M_{j,\max}} \right\}, \; k = 1, \ldots, N, \end{aligned} \tag{30}$$

with $M_{i,\max}$ as the maximum motor torque of the ith motor. Substituting Eq. (29) into Eq. (28) we get the new cost functional

$$\mathcal{L}(\mathbf{p}_B) = \frac{1}{2}\, \mathbf{e}^T\, \mathbf{W}^T\, \mathbf{W}\, \mathbf{e}\,. \tag{31}$$

Now the unknown parameters are calculated by

$$\left\{ \frac{\partial \mathcal{L}(\mathbf{p}_B)}{\partial \mathbf{p}_B} \right\}^T = \mathbf{\Theta}_B^T\, \mathbf{W}^T\, \mathbf{W}\, \mathbf{Q} - \mathbf{\Theta}_B^T\, \mathbf{W}^T\, \mathbf{W}\, \mathbf{\Theta}_B\, \mathbf{p}_B = 0, \tag{32}$$

leading to

$$\mathbf{p}_B = \left(\mathbf{\Theta}_B^T\, \mathbf{W}^T\, \mathbf{W}\, \mathbf{\Theta}_B \right)^{-1} \mathbf{\Theta}_B^T\, \mathbf{W}^T\, \mathbf{W}\, \mathbf{Q}\,. \tag{33}$$

Further information concerning experimental results is presented in Section 5.

Clearly, the trajectory which is used for the identification influences the result substantially. For a good excitation of the parameters we will obtain reliable parameters. Information about the excitation is supplied by the covariance matrix $\mathbf{\Lambda} = \mathbf{\Theta}_B^T\, \mathbf{\Theta}_B$. Hence, we assume to get a good solution by calculating a trajectory where the condition number of $\mathbf{\Lambda}$ (cond($\mathbf{\Lambda}$)) is as low as possible. Note, by a bad choice of the trajectory also the rank of the matrix $\mathbf{\Lambda}$ can decrease and thus the identification process cannot be carried out.

4.2. Optimal identification trajectory

The calculation of optimal trajectories is based on the work of ref. [21]. Each joint trajectory is defined by a Fourier series. Thus the trajectory of the ith joint is given by

$$q_i(t) = \sum_{l=1}^{N_i} \left(\frac{a_{i,l}}{\omega\, l}\, \sin(\omega\, l\, t) - \frac{b_{i,l}}{\omega\, l}\, \cos(\omega\, l\, t) \right), \tag{34}$$

and is characterized by the order N_i, the ground frequency ω, the joint offset $q_{i,0}$, and the Fourier coefficients $a_{i,l}$ and $b_{i,l}$. For simplicity, the ground frequency as well as the order N_i are predefined and identical for all seven joints. Besides, the coefficients $a_{i,l}$ are represented by the vector

$$\mathbf{a}^T = \left[a_{1,1} \; \cdots \; a_{1,N_i} \; \cdots \; a_{7,N_i} \right]^T$$

and coefficients $b_{i,l}$ are combined in

$$\mathbf{b}^T = \left[b_{1,1}, \ldots, b_{1,N_i}, \ldots, b_{7,N_i} \right]^T .$$

Note, $\mathbf{\Theta}_B$ and $\mathbf{Q}$ are evaluated for discrete values of $\mathbf{q}$, $\dot{\mathbf{q}}$, and $\ddot{\mathbf{q}}$, see Eq. (26). Thus Eq. (34) is discretized, leading to

$$q_i(k) = \sum_{l=1}^{N_i} \left(\frac{a_{i,l}}{\omega\, l}\, \sin(\omega\, l\, k\, T_s) - \frac{b_{i,l}}{\omega\, l}\, \cos(\omega\, l\, k\, T_s) \right), \tag{35}$$

https://doi.org/10.1017/S0263574714001465 Published online by Cambridge University Press

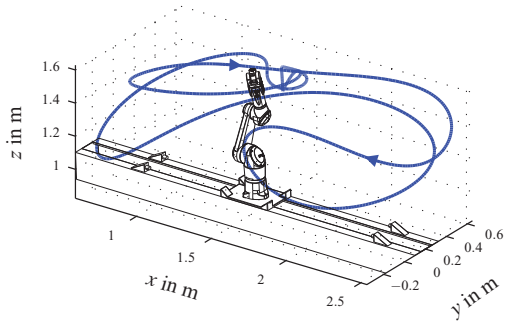

Fig. 3. End-effector path of the calculated optimal trajectory.

where k denotes the discrete time index and T_s the sampling time. Now the optimization problem follows to

$$\begin{aligned} &\min_{\mathbf{a},\mathbf{b}} \ \text{cond}(\mathbf{\Lambda}(\mathbf{q}, \dot{\mathbf{q}}, \ddot{\mathbf{q}})), \\ &\text{subject to:} \\ &\mathbf{q}_{\min} \leq \mathbf{q} \leq \mathbf{q}_{\max}, \\ &|\dot{\mathbf{q}}| \leq \dot{\mathbf{q}}_{\max}, \\ &|\ddot{\mathbf{q}}| \leq \ddot{\mathbf{q}}_{\max}, \\ &\text{no collisions,} \end{aligned} \tag{36}$$

with the mechanical joint limits $\mathbf{q}_{\min}$ and $\mathbf{q}_{\max}$, the maximum joint velocities $\dot{\mathbf{q}}_{\max}$ and maximum joint acceleration $\ddot{\mathbf{q}}_{\max}$. The solution of the optimization problem is calculated with the Matlab-Optimization-Toolbox (fmincon). Besides, for the computation the parameters $N_i = 5, \omega = 0.8\,\text{rad/s}$ and $k = 800$ are used. Also a calculation using a genetic algorithm as published in ref. [6] is possible. In Fig. 3 the end-effector path for the optimal trajectory is shown. Along the path, end-effector velocities of up to $2.7\,\text{m/s}$ and accelerations up to $11.3\,\text{m/s}^2$ appear. The corresponding joint trajectories are depicted in Fig. 4. As pointed out at the beginning of this section, the joint velocities and accelerations for the identification procedure are calculated by a filter. Hence, Fig. 5 shows a comparison of the desired and calculated joint velocities and accelerations for q_3.

5. Experimental Results

Apart from the theoretical discussion, in this section the results of the identification are presented and the addressed reliability of the dynamic parameters is highlighted. As mentioned in Section 4 the weighting of the cost functional is very important. To emphasize this, Fig. 6 shows the measured as well as the simulated motor torques for the axis 1, 5, and 7. In this figure, the simulation results are obtained by using parameters from an identification without any weighting ($\mathbf{W} = \mathbf{I}$). In comparison, Fig. 7 shows the same measurements but with simulation results, obtained with parameters from an identification with the introduced weighting of Eq. (30). Obviously, there is an evident improvement of the matching between simulation and measurement by weighting the error $\mathbf{e}$ appropriate. Most important, without any weighting, the mass matrix is not positive definite and thus the parameters represent a non-physical system. Using parameters evaluated with the weighting matrix $\mathbf{W}$ the mass matrix is as expected positive definite. In order to verify the dynamic model, the real and simulated motor torques are compared for a verification trajectory, see Fig. 9. The end-effector path of the verification trajectory is defined in the EN ISO NORM 9283, see ref. [11] and is shown in Fig. 8.

To evaluate the quality of the identification the average feed-forward torque error

$$\bar{\mathbf{e}} = \begin{bmatrix} \bar{e}_1, \ldots, \bar{e}_7 \end{bmatrix} \tag{37}$$

https://doi.org/10.1017/S0263574714001465 Published online by Cambridge University Press

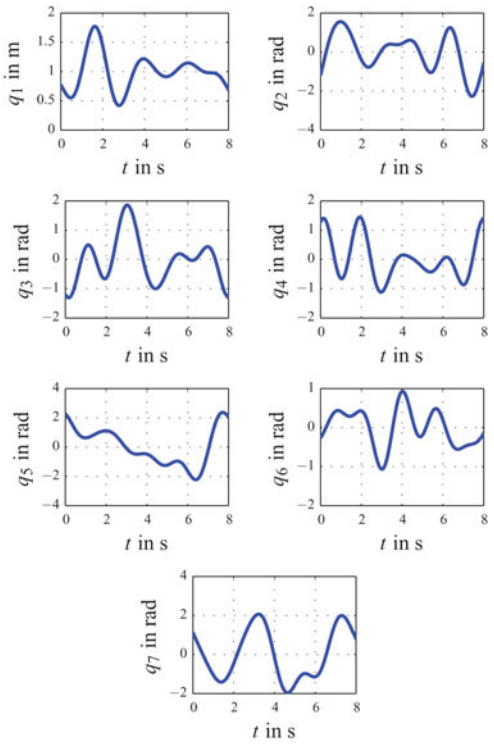

Fig. 4. Joint trajectories of the optimal trajectory.

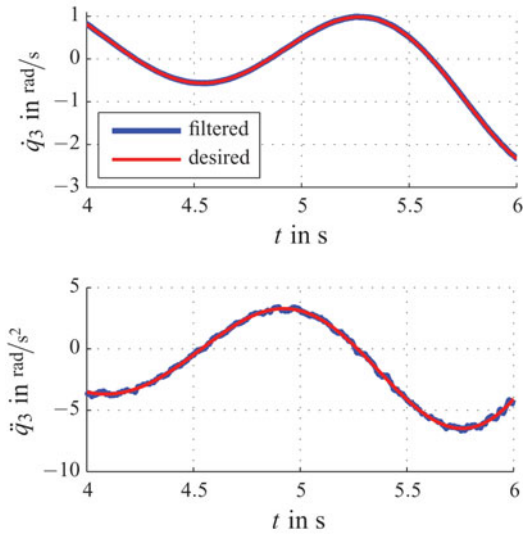

Fig. 5. Comparison of the desired and filtered joint velocities and accelerations of q_3.

with $\overline{e}_i$ the average error of $\hat{\mathbf{e}}_i$ (see Eq. (29)), whereby i indicates that only the error according to the ith axis is considered, is calculated. Figure 10 shows the error $\overline{\mathbf{e}}$ evaluated for the identification trajectory and the verification trajectory. Of course the average error of the verification trajectory is a bit higher, since, for example, stiction is not included in the model.

Nevertheless, the average error between the feed-forward calculation and the actual motor torque stays beneath 1% of the maximum motor torque. Thus, the identification worked well and an accurate model of the robot has been found.

https://doi.org/10.1017/S0263574714001465 Published online by Cambridge University Press

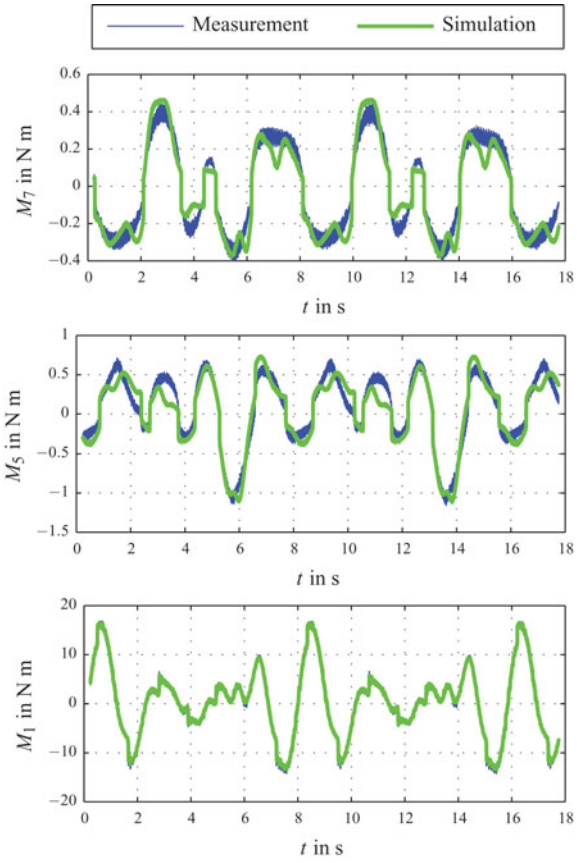

Fig. 6. Motor torque measured and simulated with the identified parameters—without weighting and for the identification trajectory.

6. Temperature Dependency of the Base Parameters

Thus far, the modeling of rigid body systems and the following identification of reliable parameters was presented. In this section, the influence of temperature changes on the dynamics and thus on the base parameters is discussed. Therefore, two identifications are performed. One for a cold robot right after start-up and one after about half an hour of high dynamic movements when the robot has reached its operating temperature. To illustrate the effects, some of the identified parameters for the cold robot are compared to the parameters identified at the operating temperature, denoted by the superscript c and w, respectively. So we get:

$$\begin{aligned}
\mathbf{p}_B^c(1) &= 273.40\,\text{kg}, & \mathbf{p}_B^w(1) &= 273.62\,\text{kg},\\
\mathbf{p}_B^c(2) &= 1.68\,\text{kg m}, & \mathbf{p}_B^w(2) &= 1.65\,\text{kg m},\\
\mathbf{p}_B^c(27) &= 248.41\,\text{Ns/m}, & \mathbf{p}_B^w(27) &= 90.19\,\text{Ns/m},\\
\mathbf{p}_B^c(28) &= 41.26\,\text{N m s}, & \mathbf{p}_B^w(28) &= 25.65\,\text{N m s},\\
\mathbf{p}_B^c(34) &= 312.50\,\text{N}, & \mathbf{p}_B^w(34) &= 233.00\,\text{N},\\
\mathbf{p}_B^c(35) &= 18.24\,\text{N m}, & \mathbf{p}_B^w(35) &= 15.07\,\text{N m}.
\end{aligned}$$

As expected, base parameters which contain effects according to inertia (e.g. $\mathbf{p}_B(1)$, $\mathbf{p}_B(2)$) remain almost the same, but the change in the friction parameters (e.g. $\mathbf{p}_B(27)$ – $\mathbf{p}_B(35)$)) is unexpectedly high. For example, the viscous friction of the linear axis decreases drastically, to 36 % of the parameter identified for the cold robot. This is due to the fact that the behavior of the used lubricant changes significantly w.r.t. temperature. Nevertheless, the results reaffirm the identification method, because

https://doi.org/10.1017/S0263574714001465 Published online by Cambridge University Press

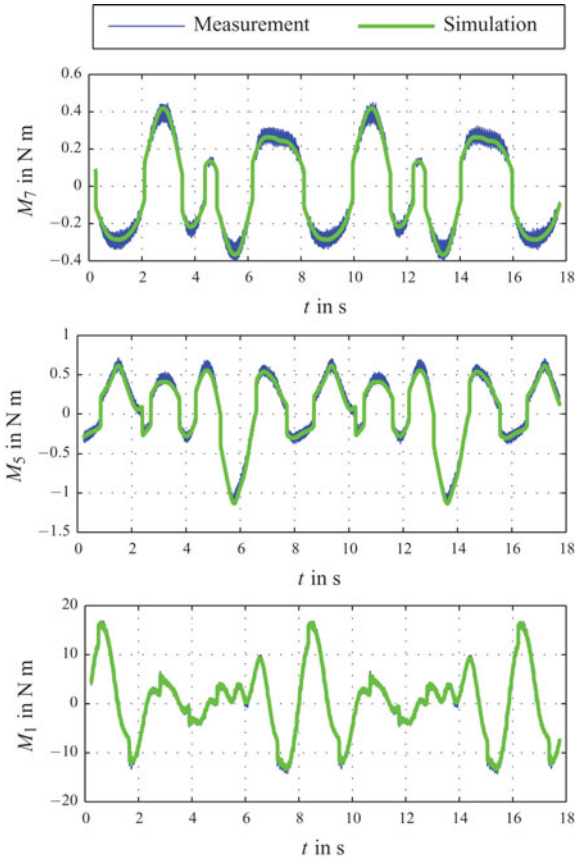

Fig. 7. Motor torque measured and simulated with the identified parameters—with weighting and for the identification trajectory.

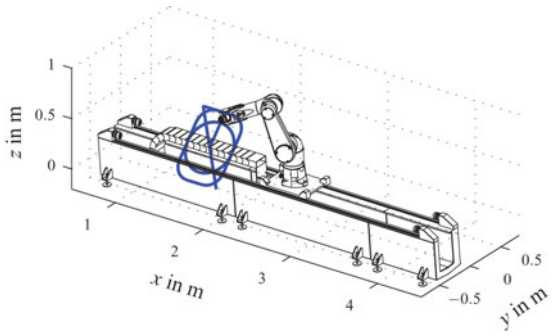

Fig. 8. End-effector path of the verification trajectory.

all parameters which are assumed to be independent from the temperature stay constant and the other ones change according to the temperature.

7. Computation Time

A side benefit of using base parameters is the reduction of the required computation time for the evaluation of the feed-forward torque (inverse dynamics). To demonstrate the benefit of base parameters w.r.t. computation time, two implementations of feed-forward calculations are compared on the real-time system of our robot. The first implementation relies on

$$\mathbf{Q}_{m,d} = \mathbf{M}(\mathbf{q}_d)\,\ddot{\mathbf{q}}_d + \mathbf{h}(\mathbf{q}_d, \dot{\mathbf{q}}_d), \tag{38}$$

https://doi.org/10.1017/S0263574714001465 Published online by Cambridge University Press

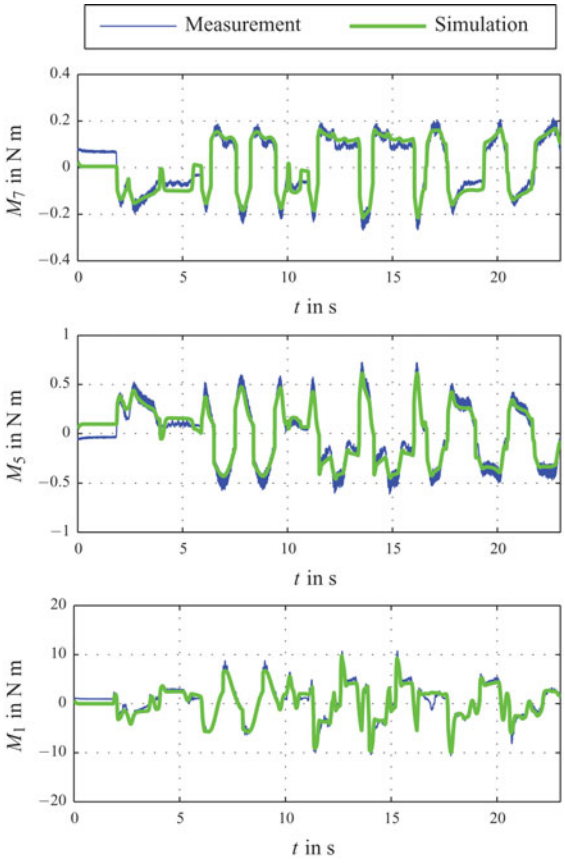

Fig. 9. Motor torque measured and simulated for the verification trajectory.

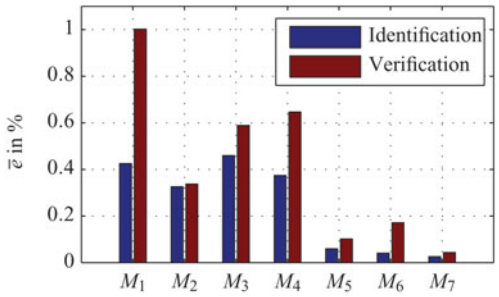

Fig. 10. Average feed-forward torque error for the identification trajectory and the verification trajectory.

with the whole set of 70 parameters. Note, $\mathbf{M}(\mathbf{q}_d)$ is the mass matrix and $\mathbf{h}(\mathbf{q}_d, \dot{\mathbf{q}}_d)$ are the nonlinear terms of our dynamic model for a desired trajectory, denoted by the index d. The second implementation uses the linear equation in the parameter range, which is also used for the parameter identification

$$\mathbf{Q}_{m,d} = \mathbf{\Theta}_B(\mathbf{q}_d, \dot{\mathbf{q}}_d, \ddot{\mathbf{q}}_d)\,\mathbf{p}_B, \tag{39}$$

with the base parameters $\mathbf{p}_B$. The calculation time for Eq. (39) was maximally 11.928 μs. In contrary, the calculation of Eq. (38) requires 15.243 μs. So, using a base parameter representation to calculate the feed-forward torque leads to a reduction of computation time of 22 %. Both feed-forward calculations were implemented on an industrial PC with 2.16 GHz.

https://doi.org/10.1017/S0263574714001465 Published online by Cambridge University Press

8. Conclusion

In this contribution we presented a direct method, based on the projection equation, for deriving a dynamic model which fulfills the requirements of the parameter identification. Furthermore, the identification and the calculation of optimal trajectories were discussed in detail and demonstrated for a seven-axes robot. The theoretical discussion was verified by experimental results and new scientific findings regarding the identification of a positive definite mass matrix were found. There the key was the enhancement of the cost functional by a weighting matrix in order to obtain physical reliable parameters. Concerning the reliability, also a verification by additional trajectories is included in this contribution. Furthermore, practical problems like temperature effects were addressed as well as the reduction of the computation time by using base parameters for a model-based feed-forward control.

Acknowledgments

This work has been partially supported by the Austrian COMET-K2 program of the Linz Center of Mechatronics (LCM), and was funded by the Austrian federal government and the federal state of Upper Austria.

References

1. A. Albu-Schäffer, Regelung von Robotern mit elastischen Gelenken am Beispiel der DLR-Leichtbauarme *Ph.D. Thesis* (München, Germany: Technische Universität München, 2002).
2. G. Antonelli, F. Caccavale and P. Chiacchio, "A systematic procedure for the identification of dynamic parameters of robot manipulators," *Robotica* **17**, 427–435 (1999).
3. A. Bejczy, "Robot arm dynamics and control," *Computer* **15**, 62–80 (1982).
4. F. Benimeli, V. Mata and F. Valero, "A comparison between direct and indirect dynamic parameter identification methods in industrial robots," *Robotica* **24**, 579–590 (2006).
5. H. Bremer, *Dynamik und Regelung mechanischer Systeme* (Teubner Studienbücher, Stuttgart, 1988).
6. G. Calafiore, M. Indri and B. Bona, "Robot dynamic calibration: Optimal excitation trajectories and experimental parameter estimation," *J. Robot. Syst.* **18**, 55–68 (2001).
7. J. Craig, *Introduction to Robotics: Mechanics and Control* (Pearson Prentice Hall, New Jersey, 2004).
8. H. Gattringer, R. Riepl and M. Neubauer, "Optimizing industrial robots for accurate high-speed applications," *J. Ind. Eng.* **2013**, 12 (2013).
9. M. Gautier, "Numerical calculation of base inertial parameters of robots," *J. Robot. Syst.* **8**, 485–506 (1991).
10. M. Gautier and W. Khalil, "Exciting Trajectories for the Identification of Base Inertial Parameters of Robots," *Proceedings of the 30th IEEE Conference on Decision and Control*, vol. 1, Brighton, England (Dec. 11–13, 1991) pp. 494–499.
11. ISO NORM 9283, Manipulating Industrial Robots—Performance and Criteria. Norm, EN ISO 9283 (1998).
12. W. Khalil and E. Dombre, *Modeling, Identification and Control of Robots* (Kogan Page Science, London, 2004).
13. W. Khalil and J. Kleinfinger, "Minimum operations and minimum parameters of the dynamic models of tree structure robots," *IEEE J. Robot. Autom.* **RA-3**(6), 517–526 (1987).
14. P. Khosla, "Categorization of parameters in the dynamic robot model," *IEEE Trans. Robot. Autom.* **5**, 261–268 (1989).
15. K. Kozlowski, *Modelling and Identification in Robotics* (Springer Verlag, London, 1998).
16. K. R. Kozlowski and P. Dutkiewicz, "Experimental identification of dynamic parameters for a class of geared robots," *Robotica* **14**, 561–574 (1996).
17. F. Pfeiffer and J. Hölzl, "Parameter Identification for Industrial Robots," *Proceedings of the 1995 IEEE International Conference on Robotics and Automation*, vol. 2, Nagoya, Aichi, Japan (May 21–27, 1991) pp. 1468–1476.
18. L. Sciavicco and B. Siciliano, *Modelling and Control of Robot Manipulators* (Springer Verlag, London, 2004).
19. B. Siciliano and O. Khatib, eds., *Handbook of Robotics* (Springer Verlag, Berlin, Heidelberg, 2008).
20. B. Siciliano, L. Sciavicco, L. Villani and G. Oriolo, *Robotics—Modelling, Planning and Control* (Springer Verlag, London, 2009).
21. J. Swevers, C. Ganseman, D. Tükel, J. D. Schutter and H. V. Brussel, "Optimal robot excitation and identification," *IEEE Trans. Robot. Autom.* **13**, 730–740 (1997).

https://doi.org/10.1017/S0263574714001465 Published online by Cambridge University Press